Journal of Scientific Computing (2026) 107:5
https://doi.org/10.1007/s10915-026-03219-6

An Efficient Spectral Method for Elliptic Interface Problems in Two-Dimensional Complex Domains

Jing An[1] · **Jie Shen**[2] · **Wei Wang**[1]

Received: 2 September 2025 / Revised: 18 January 2026 / Accepted: 6 February 2026

Abstract
We propose in this paper a new spectral method based on a fictitious domain approach for solving elliptic interface problems in complex domains. Firstly, we embed the complex domain into a larger fictitious domain whose boundary is a proportional extension of the interface. Assuming the data can be smoothly extended to the fictitious domain, we formulate a Petrov-Galerkin weak form in the fictitious domain under the constraint that its solution satisfied the original boundary condition and interface condition. Secondly, by introducing an appropriate coordinate transformation, we map the fictitious domain to a circular domain with the interface mapped to an inner circle. Thirdly, we develop an efficient Fourier-Legendre spectral method for solving the mapped equation in the circular domain. We present ample numerical examples to validate the efficiency and accuracy of our approach. In particular, our numerical results indicate that our method can achieve exponential convergence if the interface and domain boundary are smooth.

Keywords Elliptic interface problem · Complex domain · Fictitious domain approach · Spectral method

1 Introduction

Second-order elliptic interface problems have wide applications in fluid dynamics, electromagnetics, biomedicine, and materials science [2, 3, 12, 13, 21, 44, 46], particularly in reservoir simulation, seismic wave propagation, and porous media diffusion. However, the fact that the solution may exhibit singularities due to coefficient jumps (such as differences in permeability), along with the complexity of interface geometries, pose significant challenges in its numerical approximation.

✉ Jie Shen
jshen@eitech.edu.cn

Jing An
anjing@gznu.edu.cn

Wei Wang
weiwang10901@163.com

[1] School of Mathematical Sciences, Guizhou Normal University, 550025 Guiyang, China

[2] Eastern Institute of Technology, 315200 Ningbo, Zhejiang, China

Published online: 18 February 2026

Numerous numerical methods have been proposed for the second-order elliptic interface problems, including the finite element methods [5, 9], finite volume methods [15, 36, 38], and finite difference methods [4, 11, 42]. For instance, the finite element (FE) methods face challenges in mesh adaptation for complex interface scenarios; the finite volume methods suffer from accuracy degradation near interfaces; and the finite difference methods struggle to accommodate complex geometries. To overcome geometric constraints, Lin et al. introduce an immersed finite element (IFE) method and achieved mesh-independent convergence by modifying basis functions at the interface [1, 30–32]. Subsequently, this idea has been extended to immersed finite volume methods [8, 14, 20, 40] and immersed interface methods [25, 27–29].

Recently, the elliptic interface problems attracted increasing attentions. Zhang et al. [45] proposed a numerical method based on variational discretization, which address the interface optimal control problem by using a uniform grid independent of the complex interface and the immersed finite element method. Coco et al. [10] proposed a second-order accurate finite difference method with real and ghost values to address non-homogeneous jump conditions in two-dimensional and three-dimensional elliptic problems with complex interfaces. Mu et al. [33] introduce a novel weak Galerkin (WG) finite element method, by simplifying the variational form and reducing the number of unknowns, this method can efficiently solve second-order elliptic interface problems on general polyhedral meshes. Oruç [34] proposed a meshless algorithm based on Pascal polynomials and a multiscale method, by discretizing the strong form, it can effectively deal with two-dimensional and three-dimensional elliptic interface problems with sharp corner interfaces. Guo et al. [19] propose an IFE method based on Cartesian grids. They construct a local IFE space that satisfy the interface jump conditions using piecewise trilinear polynomials, thereby achieving efficient solutions for three-dimensional elliptic interface problems. Guittet et al. [18] proposed a simple algorithm, called the Voronoi interface method, for solving elliptic interface problems with discontinuities on the interfaces of irregular regions, it can achieve second-order accuracy for the solution and first-order accuracy for the gradient on arbitrary grids, and is applicable to cases with large ratio of diffusion coefficients. For additional related work, we refer to [22, 26, 35, 47].

It is well known that spectral methods can deliver superior accuracy for problems posed on regular domains with smooth solutions [6, 37], and that the spectral element method (SEM) combines the geometric flexibility of finite elements with the high precision of spectral approximations [7]. In recent years, several non-conforming least-squares spectral element methods have been proposed for solving elliptic interface problems. For instance, Kumar et al. [24] developed a least-squares based non-conforming SEM for two-dimensional elliptic problems with smooth interfaces, achieving exponential convergence in the H^1 norm through the use of a preconditioned conjugate gradient solver to correct the non-conforming solution; Khan et al. [23] extended this framework to three-dimensional elliptic interface problems. However, these approaches face significant challenges. The method in [24] requires additional correction steps to obtain a coordinated solution, which increases implementation complexity. Moreover, when coefficients exhibit large jumps, both the number of iterations and the computational cost rise sharply. Similarly, the three-dimensional method in [23] shows limited robustness in the presence of large coefficient jumps, leading to substantial iteration counts and high computational expense. In addition, the use of non-coordinated discretization and analytical mappings further complicates programming and mesh generation. Consequently, non-conforming least-squares SEMs often struggle with grid construction, computational efficiency, and numerical accuracy, particularly for elliptic problems involving heterogeneous media and complex interfaces in irregular domains.

In summary, traditional numerical methods for elliptic interface problems generally require explicit meshing of the computational domain and careful design of interface transmission conditions, which may incurs a large number of degrees of freedom and introduce additional errors due to boundary approximation. As a result, achieving high-accuracy solutions often demands significant computational resources in terms of both time and memory.

Motivated by these challenges and by the success of domain embedding approach introduced in [16, 17], we propose a novel spectral method that integrates the domain embedding approach with domain mapping. Compared to existing approaches, our method incorporates the following key innovations:

- We develop a spectral element framework based on regional embedding and mapping, applicable to problems with heterogeneous media, complex interfaces, and intricate boundaries.
- After extending the original problem to a large fictitious domain with boundary being a proportional extension of the original interface (see Fig. 1), we transform the extended problem in the complex domain into a problem in a circular domain in which Fourier-Legendre spectral methods can be efficiently applied, while enforcing the original interface conditions and boundary conditions in a Petrov–Galerkin weak formulation.
- The proposed algorithm attains spectral accuracy, requiring significantly fewer degrees of freedom to obtain highly accurate numerical solutions.

The rest of the paper is structured as follows: In Section 2, we describe the second-order elliptic interface problem. In Section 3, we extended the original problem to the fictitious domain and derived its variational form in Cartesian coordinates. In Section 4, we introduce a coordinate transformation and derive an equivalent variational form under this transformation. In Section 5, we establish a discrete variational form and describe our approach for solving the associated linear system. In Section 6, we present a series of numerical examples to validate the robustness and accuracy of approach. We provide some concluding remarks in Section 7, followed by an appendix with detailed.

2 Description of the Elliptic Interface Problem

We consider the following elliptic interface problem [9]:

$$\begin{aligned} &-\nabla\cdot(\varrho\nabla\sigma) = F, \quad \text{in } \Omega^-\cup\Omega^+,\\ &\sigma = 0, \quad \text{on } \partial\Omega,\\ &[\sigma]_\Gamma = \left[\varrho\frac{\partial\sigma}{\partial\mathbf{n}}\right]_\Gamma = 0, \end{aligned} \tag{2.1}$$

where $\Omega \in \mathbb{R}^2$ and $\Omega^- \subset \Omega$ are simply connected domains with at least piecewise C^1 boundaries; let $\Omega^+ = \Omega \setminus \bar{\Omega}^-$, and $\Gamma := \partial\Omega^- \cap \partial\Omega^+$ denotes the interface separating the subdomains Ω^- and Ω^+; hence $\Omega = \Omega^- \cup \Omega^+ \cup \Gamma$ (see left of Fig. 1). The jump conditions across the interface are as follows:

$$[\sigma]_\Gamma = \sigma|_{\Gamma^-} - \sigma|_{\Gamma^+}, \quad \left[\varrho\frac{\partial\sigma}{\partial\mathbf{n}}\right]_\Gamma = \varrho_-\frac{\partial\sigma}{\partial\mathbf{n}}\bigg|_{\Gamma^-} - \varrho_+\frac{\partial\sigma}{\partial\mathbf{n}}\bigg|_{\Gamma^+},$$

with a general non-uniform medium given by

$$\varrho(\mathbf{x}) = \begin{cases} \varrho_-(\mathbf{x}), & \mathbf{x}\in\Omega^-,\\ \varrho_+(\mathbf{x}), & \mathbf{x}\in\Omega^+. \end{cases}$$

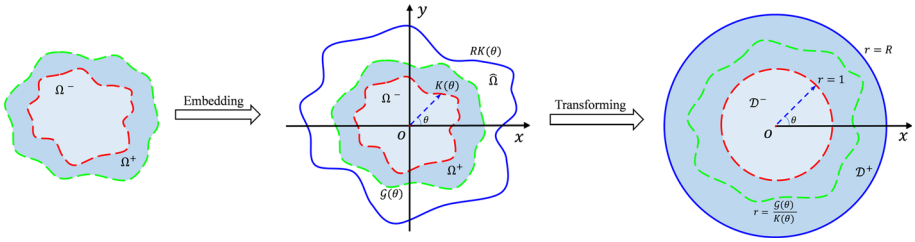

Fig. 1 The diagram of domain embedding and transformation

To fix the idea, we assume that $\partial\Omega^-$ and $\partial\Omega$ can be parametrized by $K(\theta)$ and $\mathcal{G}(\theta)$, $\theta \in [0, 2\pi)$, respectively. Therefore

$$\begin{aligned}
\Omega &:= \{\mathbf{x} \in \mathbb{R}^2 : |\mathbf{x}| < \mathcal{G}(\theta),\ \theta \in [0, 2\pi)\},\\
\Omega^- &:= \{\mathbf{x} \in \mathbb{R}^2 : |\mathbf{x}| < K(\theta),\ \theta \in [0, 2\pi)\},\\
\Omega^+ &:= \{\mathbf{x} \in \mathbb{R}^2 : K(\theta) < |\mathbf{x}| < \mathcal{G}(\theta),\ \theta \in [0, 2\pi)\}.
\end{aligned}$$

3 Domain Embedding and Variational form in the Cartesian Coordinate System

First, we choose $R > 1$ such that $RK(\theta) \geq \mathcal{G}(\theta)$ for all $\theta \in [0, 2\pi)$, and denote:

$$\begin{aligned}
\hat{\Omega} &= \{\mathbf{x} \in \mathbb{R}^2 : |\mathbf{x}| < RK(\theta),\ \theta \in [0, 2\pi)\},\ \hat{\Omega}^- = \Omega^-,\\
\hat{\Omega}^+ &= \{\mathbf{x} \in \mathbb{R}^2 : K(\theta) < |\mathbf{x}| < RK(\theta),\ \theta \in [0, 2\pi)\}.
\end{aligned}$$

Next, we extend the original problem (2.1) from Ω to $\hat{\Omega}$:

$$\begin{aligned}
&-\nabla \cdot (\varepsilon \nabla \delta) = \mathcal{F}, \quad \text{in } \hat{\Omega}^- \cup \hat{\Omega}^+,\\
&\delta = 0, \quad \text{on } \partial\Omega,\\
&[\delta]_\Gamma = \left[\varepsilon \frac{\partial \delta}{\partial \mathbf{n}}\right]_\Gamma = 0,
\end{aligned} \tag{3.1}$$

where $\mathcal{F}$ is a smooth extension of F to $\hat{\Omega}$, $\varepsilon(\mathbf{x}) > \varrho_0 > 0$ is a general non-uniform medium, and

$$\varepsilon(\mathbf{x}) = \begin{cases} \varrho_-(\mathbf{x}), & \mathbf{x} \in \hat{\Omega}^-,\\ \varrho_+(\mathbf{x}), & \mathbf{x} \in \hat{\Omega}^+, \end{cases}$$

where we also assume that $\varrho_+(\mathbf{x})$ is smoothly extended to $\hat{\Omega}^+$.

Let $L^2(\hat{\Omega})$ and $H^1(\hat{\Omega})$ denote the standard Sobolev spaces, with their inner products and norms defined as outlined below:

$$\begin{aligned}
&(\varpi, v) = \int_{\hat{\Omega}} \varpi\, v\, d\mathbf{x},\ \ \|\varpi\| = \sqrt{(\varpi, \varpi)};\\
&(\varpi, v)_1 = (\nabla\varpi, \nabla v) + (\varpi, v),\ \ \|\varpi\|_1 = \sqrt{(\varpi, \varpi)_1}.
\end{aligned}$$

By employing Green's formula, interface transmission conditions and boundary condition, we can derive a weak form of (3.1), namely, find $\delta \in H^1(\hat{\Omega})$ such that

$$\begin{cases} \mathbb{H}(\delta, \nu) = \mathbb{Y}(\nu), \quad \forall \nu \in H_0^1(\hat{\Omega}), \\ \delta = 0, \quad \text{on } \partial\Omega, \end{cases} \tag{3.2}$$

where

$$\mathbb{H}(\delta, \nu) = \int_{\hat{\Omega}^-} \varrho_- \nabla\delta\nabla\nu d\mathbf{x} + \int_{\hat{\Omega}^+} \varrho_+ \nabla\delta\nabla\nu d\mathbf{x}, \ \mathbb{Y}(\nu) = \int_{\hat{\Omega}} \mathcal{F}\nu d\mathbf{x}.$$

4 Domain Mapping and Equivalent Variational Form

Based on the work in references [39, 41, 43], we similarly introduce the following coordinate transformation:

$$x = rK(\theta)\cos\theta, \ y = rK(\theta)\sin\theta, \ (r, \theta) \in [0, R) \times [0, 2\pi), \tag{4.1}$$

which transforms the complex domains Ω^- and $\hat{\Omega}$ into regular domains $\mathcal{D}^-$ and $\mathcal{D}$ (see Fig. 1):

$$\begin{aligned} \mathcal{D} &:= \{(r, \theta) : (r, \theta) \in [0, R) \times [0, 2\pi)\}, \\ \mathcal{D}^- &:= \{(r, \theta) : (r, \theta) \in [0, 1) \times [0, 2\pi)\}, \\ \mathcal{D}^+ &:= \{(r, \theta) : (r, \theta) \in (1, R) \times [0, 2\pi)\}, \\ \mathcal{D}^* &:= \{(r, \theta) : (r, \theta) \in (1, \mathcal{G}(\theta)/K(\theta)) \times [0, 2\pi)\}. \end{aligned}$$

Note that after the transform, the boundary of the original domain Ω is still a complex curve, that is, $r = \frac{\mathcal{G}(\theta)}{K(\theta)}, \theta \in [0, 2\pi)$ (see Fig. 1).

Utilizing the transformation (4.1) and the chain rule, we derive that

$$\begin{aligned} \frac{\partial}{\partial x} &= \left(\frac{\cos\theta}{K(\theta)} + \frac{\sin\theta}{K^2(\theta)}\partial_\theta K(\theta)\right)\frac{\partial}{\partial r} - \frac{\sin\theta}{rK(\theta)}\frac{\partial}{\partial\theta}, \\ \frac{\partial}{\partial y} &= \left(\frac{\sin\theta}{K(\theta)} - \frac{\cos\theta}{K^2(\theta)}\partial_\theta K(\theta)\right)\frac{\partial}{\partial r} + \frac{\cos\theta}{rK(\theta)}\frac{\partial}{\partial\theta}. \end{aligned}$$

Through direct calculation, we obtain that the Jacobian determinant for the coordinate transformation (4.1) is:

$$|J(r, \theta)| = rK^2(\theta).$$

For the sake of brevity, we introduce:

$$\begin{aligned} \xi_1(\theta) &= \frac{\cos\theta}{K(\theta)} + \frac{\sin\theta}{K^2(\theta)}\partial_\theta K(\theta), \ \zeta_1(\theta) = \frac{\sin\theta}{rK(\theta)}; \\ \xi_2(\theta) &= \frac{\sin\theta}{K(\theta)} - \frac{\cos\theta}{K^2(\theta)}\partial_\theta K(\theta), \ \zeta_2(\theta) = \frac{\cos\theta}{rK(\theta)}. \end{aligned}$$

Then, we define the following weighted Sobolev spaces:

$$\begin{aligned} L^2_*(\mathcal{D}) &:= \left\{p : \int_{\mathcal{D}} rK^2(\theta)p^2 dr d\theta < \infty\right\}; \\ H^1_\star(\mathcal{D}) &:= \Big\{p : \int_{\mathcal{D}} rK^2(\theta)[(\xi_1^2 + \xi_2^2)(\partial_r p)^2 + 2(\xi_2\zeta_2 - \xi_1\zeta_1)\partial_r p\partial_\theta p \\ &\quad + (\zeta_1^2 + \zeta_2^2)(\partial_\theta p)^2 + p^2]dr d\theta < \infty, \partial_\theta p(0, \theta) = 0, p(r, \theta) = p(r, \theta + 2\pi)\Big\}; \end{aligned}$$

endowed with the inner products and norms:

$$(p,\vartheta)_* = \int_{\mathcal{D}} rK^2(\theta) p\vartheta dr d\theta,\ \|p\|_* = [(p,p)_*]^{\frac{1}{2}};$$
$$(p,\vartheta)_{1,\star} = \int_{\mathcal{D}} rK^2(\theta)[(\xi_1^2+\xi_2^2)\partial_r p\partial_r\vartheta + (\xi_2\zeta_2-\xi_1\zeta_1)(\partial_r p\partial_\theta\vartheta + \partial_\theta p\partial_r\vartheta) + (\zeta_1^2+\zeta_2^2)\partial_\theta p\partial_\theta\vartheta + p\vartheta]dr d\theta,\ \|p\|_{1,\star} = \big[(p,p)_{1,\star}\big]^{\frac{1}{2}}.$$

We also set $H^1_{0,\star}(\mathcal{D}) := \big\{p \in H^1_\star(\mathcal{D}) : p(R,\theta) = 0\big\}$, and denote

$$\hat{\varepsilon}_-(r,\theta) = \varrho_-(\mathbf{x}),\ \hat{\varepsilon}_+(r,\theta) = \varrho_+(\mathbf{x}),\ \hat{\delta}(r,\theta) = \delta(\mathbf{x}),\ \hat{\mathcal{F}}(r,\theta) = \mathcal{F}(\mathbf{x}). \tag{4.2}$$

Then, the problem (3.2) can be reformulated as: Find $\hat{\delta} \in H^1_\star(\mathcal{D})$ such that

$$\begin{cases} \hat{\mathbb{H}}(\hat{\delta},\vartheta) = \hat{\mathbb{Y}}(\vartheta),\ \forall\vartheta \in H^1_{0,\star}(\mathcal{D}), \\ \hat{\delta}(\frac{\mathcal{G}(\theta)}{K(\theta)},\theta) = 0, \quad \forall\theta \in [0,2\pi), \end{cases} \tag{4.3}$$

where

$$\hat{\mathbb{H}}(\hat{\delta},\vartheta) = \int_{\mathcal{D}^-} rK^2(\theta)\hat{\varepsilon}_-\big[(\xi_1^2+\xi_2^2)\partial_r\hat{\delta}\partial_r\vartheta + (\xi_2\zeta_2-\xi_1\zeta_1)(\partial_r\hat{\delta}\partial_\theta\vartheta + \partial_\theta\hat{\delta}\partial_r\vartheta) + (\zeta_1^2+\zeta_2^2)\partial_\theta\hat{\delta}\partial_\theta\vartheta\big]dr d\theta + \int_{\mathcal{D}^+} rK^2(\theta)\hat{\varepsilon}_+\big[(\xi_1^2+\xi_2^2)\partial_r\hat{\delta}\partial_r\vartheta + (\xi_2\zeta_2-\xi_1\zeta_1)(\partial_r\hat{\delta}\partial_\theta\vartheta + \partial_\theta\hat{\delta}\partial_r\vartheta) + (\zeta_1^2+\zeta_2^2)\partial_\theta\hat{\delta}\partial_\theta\vartheta\big]dr d\theta,$$
$$\hat{\mathbb{Y}}(\vartheta) = \int_{\mathcal{D}} rK^2(\theta)\hat{\mathcal{F}}\vartheta dr d\theta.$$

5 Discrete Variational form and its Algorithm Description

5.1 Equivalent Linear System

Firstly, we construct a set of basis functions in the approximation space. Let

$$r = \begin{cases} \frac{t_1+1}{2}, & r \in (0,1),\ t_1 \in (-1,1), \\ \frac{(R-1)t_2+R+1}{2}, & r \in (1,R),\ t_2 \in (-1,1), \end{cases} \tag{5.1}$$

and

$$\Phi_k(\varsigma) = L_k(\varsigma) - L_{k+2}(\varsigma),\ 0 \le k \le N-2,$$

where $L_k(\varsigma)$ denotes the Legendre polynomial of degree k.

Define the internal basis functions:

$$\Phi_{1,k}(r) = \begin{cases} \Phi_k(t_1(r)), & r \in (0,1), \\ 0, & r \in (1,R), \end{cases} \quad \Phi_{2,k}(r) = \begin{cases} 0, & r \in (0,1), \\ \Phi_k(t_2(r)), & r \in (1,R), \end{cases}$$

$$\Phi_{1,N-1}(r) = \begin{cases} 1-r, & r \in (0,1), \\ 0, & r \in (1,R), \end{cases} \quad \Phi_{2,N-1}(r) = \begin{cases} 0, & r \in (0,1), \\ \frac{r-1}{R-1}, & r \in (1,R), \end{cases}$$

and interface basis function:

$$\Phi_*(r) = \begin{cases} r, & r \in (0,1), \\ \frac{r-R}{1-R}, & r \in (1,R). \end{cases}$$

Denote

$$\begin{aligned} \mathbb{X}_{1N}^M &:= \text{span}\left\{\Phi_{1,k}e^{im\theta} : |m| \le M, k = 0,1,\ldots,N-1-sign(|m|)\right\}, \\ \mathbb{X}_{2N}^M &:= \text{span}\left\{\Phi_{2,k}e^{im\theta} : |m| \le M, k = 0,1,\ldots,N-2\right\}, \\ \mathbb{X}_{3N}^M &:= \text{span}\left\{\Phi_* e^{im\theta} : |m| \le M\right\},\ \mathbb{X}_{4N}^M := \text{span}\left\{\Phi_{2,N-1}e^{im\theta} : |m| \le M\right\}. \end{aligned} \tag{5.2}$$

Define two finite element approximation spaces as follows:

$$X_{MN} := \mathbb{X}_{1N}^M \oplus \mathbb{X}_{2N}^M \oplus \mathbb{X}_{3N}^M,\ \hat{X}_{MN} := \mathbb{X}_{1N}^M \oplus \mathbb{X}_{2N}^M \oplus \mathbb{X}_{3N}^M \oplus \mathbb{X}_{4N}^M.$$

Then, a discrete scheme of (4.3) reads: Find $\hat{\delta}_{MN} \in \hat{X}_{MN}$, such that

$$\begin{cases} \hat{\mathbb{H}}(\hat{\delta}_{MN}, \vartheta_{MN}) = \hat{\mathbb{Y}}(\vartheta_{MN}),\ \forall \vartheta_{MN} \in X_{MN}, \\ \int_0^{2\pi} \hat{\delta}_{MN}(\frac{G(\theta)}{K(\theta)}, \theta)e^{-in\theta}d\theta = 0,\ |n| \le M. \end{cases} \tag{5.3}$$

Using the basis functions defined in (5.2), the above discrete scheme can be reduced to a linear system

$$A\bar{u} = \bar{f}, \tag{5.4}$$

where A is the stiffness matrix associated to the linear system (5.4), $\bar{u}$ is the unknown vector whose elements are the expansion coefficients of $\hat{\delta}_{MN}$, and $\bar{f}$ is the right side vector. For the reader's convenience, the detailed description and entries of A, $\bar{u}$ and $\bar{f}$ are provided in the Appendix. Since (5.3) is a Petrov-Galerkin formulation, A is not symmetric positive definite.

Evidently, when the medium ε is piecewise constant, the coefficient matrix of system (5.4) exhibits sparse characteristics due to the orthogonality of the Legendre polynomials [37]. Consequently, we can efficiently solve the linear system (5.4) by using fast sparse solvers. When ε represents a general non-uniform medium, the coefficient matrix of system (5.4) is no longer a sparse matrix. Its elements can be accurately computed using the Gaussian-Legendre quadrature. In this case, we can solve (5.4) efficiently by employing the Preconditioned Biconjugate Gradient Stabilized method (PBiCGSTAB).

To improve the efficiency of the iterative solver, it is crucial to ensure that the preconditioning system maintains sparsity while ensuring the condition number of the preconditioned system relatively small. This can be achieved by replacing the variable coefficients in (5.3) with suitable constant coefficients so that the resulted linear system will be sparse and has similar spectral properties as the original problem. To this end, we set

$$\tilde{\varepsilon}_- = \frac{\int_{\mathcal{D}^-} rK^2(\theta)\hat{\varepsilon}_- dr d\theta}{\pi},\ \tilde{\varepsilon}_+ = \frac{\int_{\mathcal{D}^+} rK^2(\theta)\hat{\varepsilon}_+ dr d\theta}{\pi(R^2-1)},$$

and consider the following discrete scheme: Find $\tilde{\delta}_{MN} \in \hat{X}_{MN}$ such that

$$\begin{cases} \tilde{\mathbb{H}}(\tilde{\delta}_{MN}, \tilde{\vartheta}_{MN}) = \tilde{\mathbb{Y}}(\tilde{\vartheta}_{MN}),\ \forall \tilde{\vartheta}_{MN} \in X_{MN}, \\ \int_0^{2\pi} \tilde{\delta}_{MN}(\frac{G(\theta)}{K(\theta)}, \theta)e^{-in\theta}d\theta = 0,\ |n| \le M, \end{cases} \tag{5.5}$$

where

$$\begin{aligned} \tilde{\mathbb{H}}(\tilde{\delta}, \tilde{\vartheta}) = &\int_{\mathcal{D}^-} r\tilde{\varepsilon}_-\left[\partial_r\tilde{\delta}\partial_r\tilde{\vartheta} + \frac{1}{r^2}\partial_\theta\tilde{\delta}\partial_\theta\tilde{\vartheta}\right]dr d\theta + \int_{\mathcal{D}^+} r\tilde{\varepsilon}_+\left[\partial_r\tilde{\delta}\partial_r\tilde{\vartheta}\right. \\ &\left. + \frac{1}{r^2}\partial_\theta\tilde{\delta}\partial_\theta\tilde{\vartheta}\right]dr d\theta,\ \tilde{\mathbb{Y}}(\tilde{\vartheta}) = \int_{\mathcal{D}} r\tilde{\mathcal{F}}\tilde{\vartheta} dr d\theta. \end{aligned}$$

The above weak formulation leads to a linear system $B\bar{u} = \bar{f}$ with B being sparse. It is noteworthy that the interfacial transmission conditions and boundary constraints employed in (5.5) are identical to those in (5.3). This ensures that the primary characteristics of the original problem are essentially preserved. Therefore, we choose B as the preconditioner for A.

6 Numerical Experiments

In this section, we present a series of numerical examples to validate the algorithm's effectiveness.

We first describe the discrete norms which will be used to measure the errors. Let $\theta_i = \frac{2\pi i}{n}$, $i = 0, 1, \ldots, n-1$, and t_j, $j = 1, 2, \ldots, N$ be the standard Legendre-Gauss points in $[-1, 1]$. We set

$$r_{1j} = \frac{t_j + 1}{2}, \; r_{2j} = \frac{(R-1)t_j + R + 1}{2}.$$

We define the discrete $L^\infty(\mathcal{D})$ norm as follows:

$$\|f\|_{L^\infty(\mathcal{D})} = \sup_{(r_{kj}, \theta_i) \in \tilde{\mathcal{D}}} |f(r_{kj}, \theta_i)|,$$

where

$$\tilde{\mathcal{D}} := \{(r_{kj}, \theta_i) : i = 0, 1, \ldots, n-1, \; j = 1, 2, \ldots, N, \; k = 1, 2\}.$$

Similarly, we can define the discrete $L^2(\mathcal{D})$ and $H^1(\mathcal{D})$ norms.

To facilitate comparison, we utilize Example 1 from [45] as our first numerical example. Note that the interface in Example 1 is circular and the medium is piecewise constant, so the coefficient matrix A is sparse and can be efficiently inverted without a preconditioner.

6.1 Examples with Solutions which are Smooth in Ω^- and Ω^+

We present in this subsection several examples with solutions which are smooth in Ω^- and Ω^+ but are not smooth across interfaces.

Example 1 We first consider the original problem (2.1). We assign $\varrho_- = 1$, $\varrho_+ = 1000$, $R = 3$, and choose the following exact solution that satisfies both the boundary and interface conditions:

$$\sigma(x, y) = \begin{cases} (x^2 + y^2 - 0.25)(x^2 - 1)(y^2 - 1)/\varrho_-, & (x, y) \in \Omega^-, \\ (x^2 + y^2 - 0.25)(x^2 - 1)(y^2 - 1)/\varrho_+, & (x, y) \in \Omega^+, \end{cases} \tag{6.1}$$

where Ω^-, Ω^+ and the virtual domain are depicted in the left of Fig. 2.

Through coordinate transformation (4.1), we can rewritten (6.1) as:

$$\hat{\delta}(r, \theta) = \begin{cases} (r^2K^2(\theta) - K^2(\theta))(r^2K^2(\theta)\cos^2\theta - 1)(r^2K^2(\theta)\sin^2\theta - 1)/\hat{\varepsilon}_-, & (r, \theta) \in \mathcal{D}^-, \\ (r^2K^2(\theta) - K^2(\theta))(r^2K^2(\theta)\cos^2\theta - 1)(r^2K^2(\theta)\sin^2\theta - 1)/\hat{\varepsilon}_+, & (r, \theta) \in \mathcal{D}^*, \end{cases}$$

where $K(\theta) = 0.5$ and $\hat{\varepsilon}_\pm$ is given by (4.2).

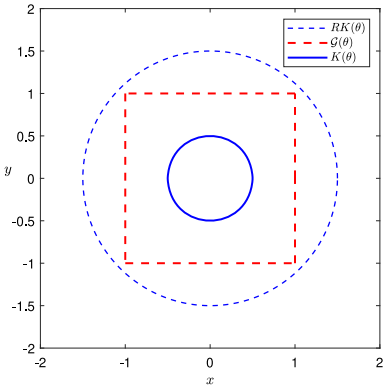

Fig. 2 Diagram illustrating the relationship between the circular interface, square boundary, and virtual boundary

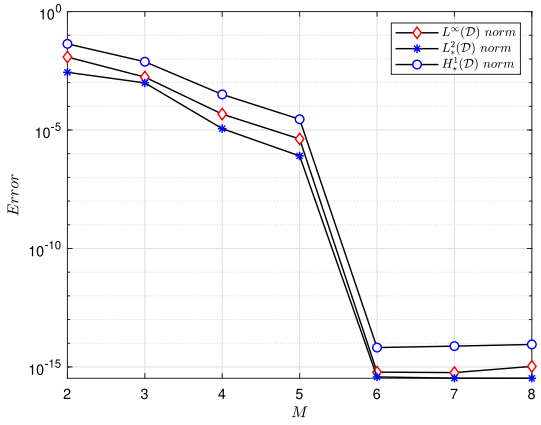

Fig. 3 Error curves under various norms for different values of M and $N = M$

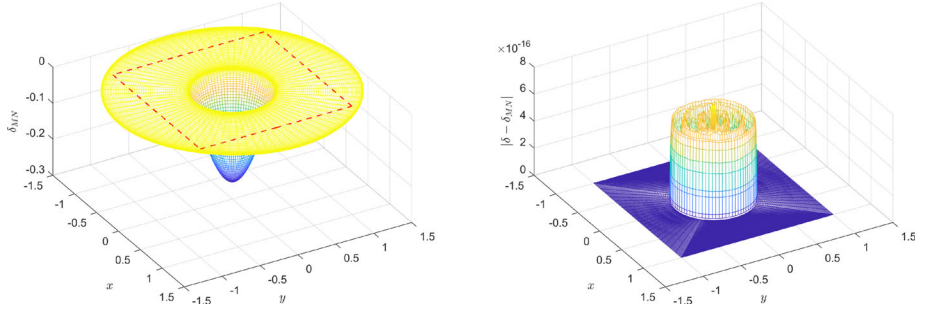

Fig. 4 Plot of approximate solution $\delta_{MN}(x, y)$ (left) and error (right) with $N = 8$ and $M = 8$

We depict the geometry of the problem in Fig. 2, plot the error curves under various norms for different values of M and $N = M$ in Fig. 3 from which the exponentially convergence is clearly observed.

In Fig. 4, we present the plot of approximate solution and error (right) with $N = 8$ and $M = 8$.

For the sake of comparison, we present the errors of approximation solutions under various norms in Tables 1 and 2 for both the spectral method and the IFE method proposed in [45].

Table 1 Errors in the L^2-norm

	IFE method	Spectral method			
h	$\|u-u_h\|_{L^2}$	Order	N	M	$\|\hat{\delta}-\hat{\delta}_{MN}\|_*$
1/8	5.1370E−03	–	3	3	9.7560E−04
1/16	1.3368E−03	1.94	4	4	1.1422E−05
1/32	3.0153E−04	2.14	5	5	8.0657E−07
1/64	6.4095E−05	2.23	6	6	3.7828E−16
1/128	1.3788E−05	2.21	7	7	3.3545E−16

Table 2 Errors in the H^1-norm

	IFE method	Spectral method			
h	$\|u-u_h\|_{1,h}$	Order	N	M	$\|\hat{\delta}-\hat{\delta}_{MN}\|_{1,\star}$
1/8	1.0446E−01	–	3	3	7.6000E−03
1/16	4.4963E−02	1.21	4	4	3.1770E−04
1/32	2.1327E−02	1.07	5	5	2.8544E−05
1/64	1.0345E−02	1.04	6	6	6.5754E−15
1/128	5.1766E−03	0.99	7	7	7.5568E−15

From Tables 1 and 2, it is obvious that, for this problem with solution that is smooth in Ω^- and Ω^+ but discontinuous at the interface, our method converges exponentially.

For the sake of brevity, the reference solutions for the next three examples are presented in polar coordinates.

Example 2 We assign $\hat{\varepsilon}_- = 1$, $\hat{\varepsilon}_+ = 1000$, $R = 3$, and choose the following exact solution that satisfies both the boundary and interface transmission conditions:

$$\hat{\delta}(r,\theta) = \begin{cases} r(r-1)(r-\frac{\mathcal{G}(\theta)}{K(\theta)})/\frac{\hat{\varepsilon}_-}{K(\theta)}, & (r,\theta)\in\mathcal{D}^-; \\ r(r-1)(r-\frac{\mathcal{G}(\theta)}{K(\theta)})/\frac{\hat{\varepsilon}_+}{K(\theta)}, & (r,\theta)\in\mathcal{D}^*, \end{cases}$$

where

$$K(\theta) = e^{\sin\theta} + e^{\cos\theta} - \sin\theta,\ \mathcal{G}(\theta) = 3.6 + 0.8\cos\theta + 0.2\sin 4\theta.$$

We plot the interface, boundary and the virtual domain in Fig. 5, and the errors under various norms for different values of M and N in Fig. 6. An exponential convergence is also observed for this example.

In Fig. 7 we plot the approximate solution (left) and error (right) with $N = M = 12$.

To examine the stability and convergence of the iterative algorithm (PBiCGSTAB), we have specifically presented the errors between the approximate solution and the reference solution for various iteration counts, as well as different values of M and N in Table 3.

From the numerical results presented in Table 3, we observe that the PBiCGSTAB algorithm demonstrates remarkable stability and rapid convergence speed in solving the system A.4.

Example 3 Let $K(\theta) = 0.65 + 0.1\sin 6\theta$, $\mathcal{G}(\theta) = 1.2 + 0.3\cos 3\theta$. We set $\hat{\varepsilon}_- = rK(\theta)\cos^2\theta$, $\hat{\varepsilon}_+ = 1000rK(\theta)\sin^2\theta$, $R = 3$, and choose the following exact solution

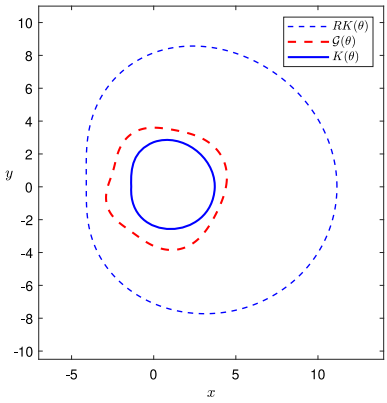

Fig. 5 Diagram illustrating the relationship between the complex interface, boundary, and virtual boundary

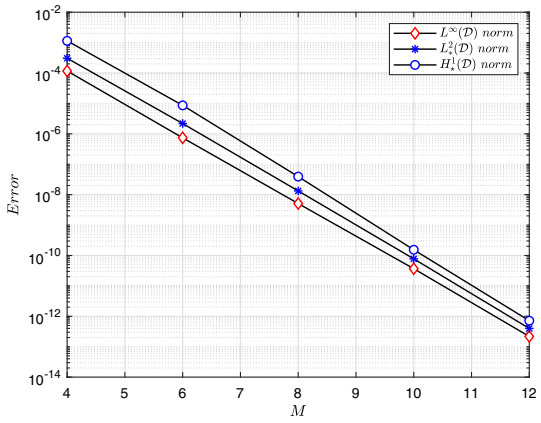

Fig. 6 Error curves under various norms for different values of M and $N = M$

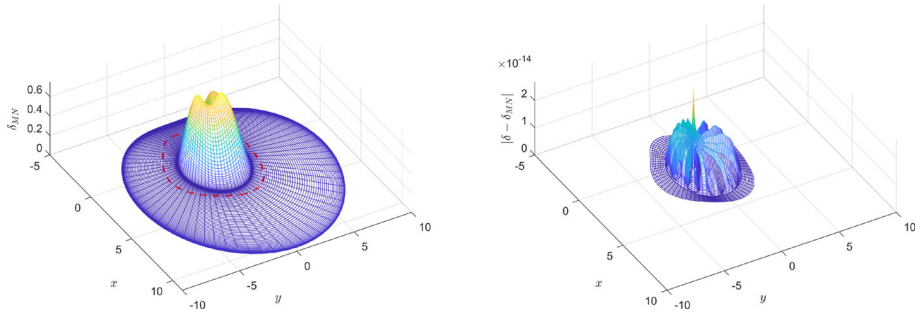

Fig. 7 The approximate solution $\delta_{MN}(x, y)$ (left) and the error with $N = 12$ and $M = 12$

that satisfies both the boundary and interface transmission conditions:

$$\hat{\delta}(r,\theta) = \begin{cases} \frac{r^4(r-1)^4}{R^4(R-1)^4}(r - \frac{\mathcal{G}(\theta)}{K(\theta)})\hat{\varepsilon}_+(1,\theta), & (r,\theta) \in \mathcal{D}^-; \\ \frac{r^4(r-1)^4}{R^4(R-1)^4}(r - \frac{\mathcal{G}(\theta)}{K(\theta)})\hat{\varepsilon}_-(1,\theta), & (r,\theta) \in \mathcal{D}^*. \end{cases}$$

Compared to Examples 1 and 2, this problem has a more complex interface. We plot the problem geometries in Fig. 8, and the errors under various norms for different values of

Table 3 Error under the $L^{\infty}(\mathcal{D})$ norm for various values of $N = M$ and iteration counts

N	Number of PBiCGSTAB iterations					
	5	10	15	20	25	30
6	5.9050E−05	7.3993E−07	7.3991E−07	7.3991E−07	7.3991E−07	7.3991E−07
8	7.4628E−05	1.6824E−08	5.1768E−09	5.1768E−09	5.1768E−09	5.1768E−09
10	2.1000E−03	6.2259E−07	5.8852E−10	3.5744E−11	3.5744E−11	3.5744E−11
12	2.4000E−03	3.6962E−06	3.9093E−10	2.1601E−13	2.1545E−13	2.1546E−13
14	7.6000E−03	3.4234E−05	2.0236E−09	1.9433E−11	2.1983E−13	2.1975E−13

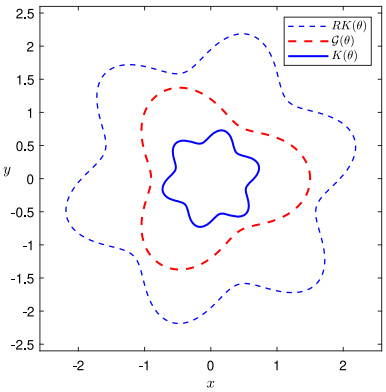

Fig. 8 Diagram illustrating the relationship between the complex interface, boundary, and virtual boundary

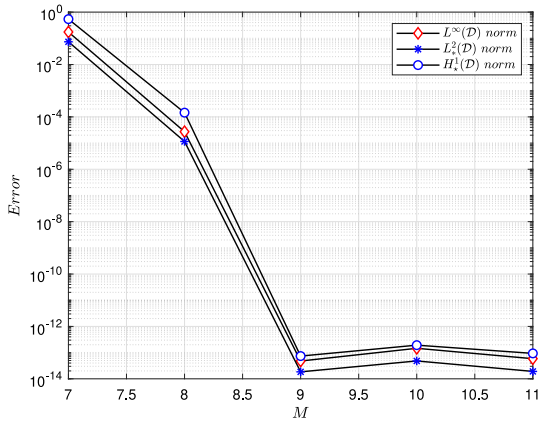

Fig. 9 Error curves under various norms for different values of M and $N = M$

M and N in Fig. 9. It is clear that an exponential convergence is also achieved for this example.

In Fig. 10 we plot the approximate solution (left) and error (right) with $N = M = 10$.

6.2 Examples with Solutions Having Limited Regularities in Ω^- and Ω^+

In this subsection, we present two examples where the solutions only have limited regularities in Ω^- and Ω^+.

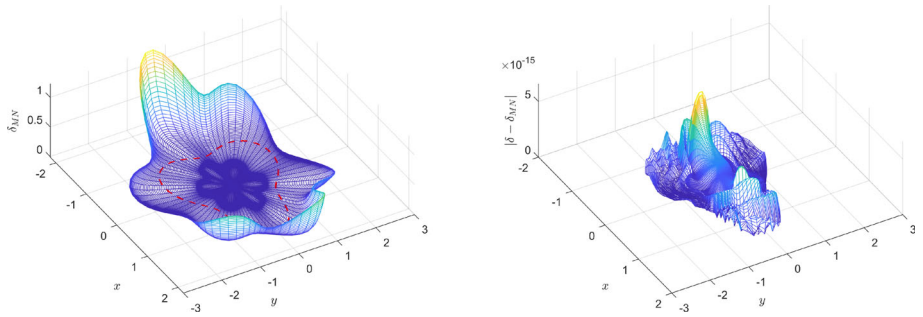

Fig. 10 Approximate solution $\delta_{MN}(x, y)$ (left), and error with (10, 10) (right)

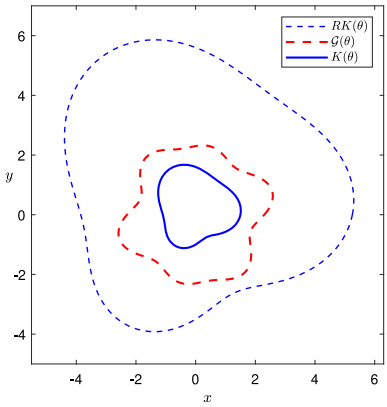

Fig. 11 Diagram illustrating the relationship between the complex interface, boundary, virtual boundary

Example 4 We assign $\hat{\varepsilon}_- = 1$, $\hat{\varepsilon}_+ = 10000$, $R = 3.5$, and choose the following as the exact solution which satisfies both the boundary and interface transmission conditions:

$$\hat{\delta}(r,\theta) = \begin{cases} r^2(|r-0.7|^5 + |r-1.2|^5)(r-1)(r-\frac{\mathcal{G}(\theta)}{K(\theta)})/\frac{\hat{\varepsilon}_-}{K(\theta)}, & (r,\theta) \in \mathcal{D}^-; \\ r^2(|r-0.7|^5 + |r-1.2|^5)(r-1)(r-\frac{\mathcal{G}(\theta)}{K(\theta)})/\frac{\hat{\varepsilon}_+}{K(\theta)}, & (r,\theta) \in \mathcal{D}^*, \end{cases}$$

where

$$K(\theta) = 1.3 + 0.3\sin\theta + 0.2\cos 3\theta, \ \mathcal{G}(\theta) = 2.3 + 0.4\cos\theta\sin 5\theta.$$

We plot the problem geometries in Fig. 11, and the errors under various norms for different values of M and N in log-log scale Fig. 12. We observe that for this example, our algorithm only leads to algebraic convergence rate due to the limited regularity in each subdomain.

In addition, we present the images of the reference solution and its approximate solution in Fig. 13.

Example 5 In the previous examples, all solutions are explicitly given. For this final example, we choose the right-hand side of equation (2.1) $F = 1$, and set $\hat{\varepsilon}_- = 0.01$, $\hat{\varepsilon}_+ = 0.1$, and $R = 1.5$. The interface and the outer boundary are specified in polar coordinates by

$$K(\theta) = 1.8 + e^{0.3\cos 3\theta}, \ \mathcal{G}(\theta) = 2.5 + e^{0.2\sin 3\theta},$$

respectively. Due to the choice of F and the difference between $\hat{\varepsilon}_-$ and $\hat{\varepsilon}_+$, the unknown solution only has very limited regularity.

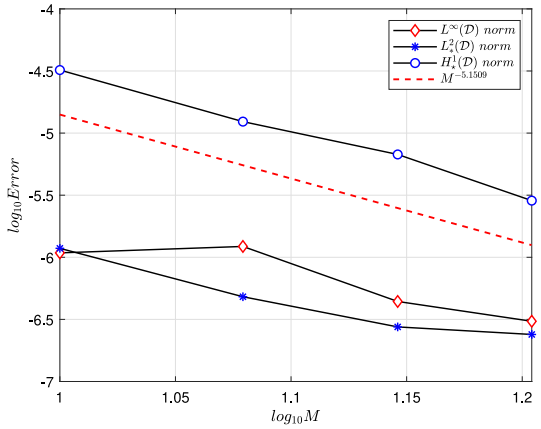

Fig. 12 Error curves under various norms on a log-log scale for different values of M and $N = M$

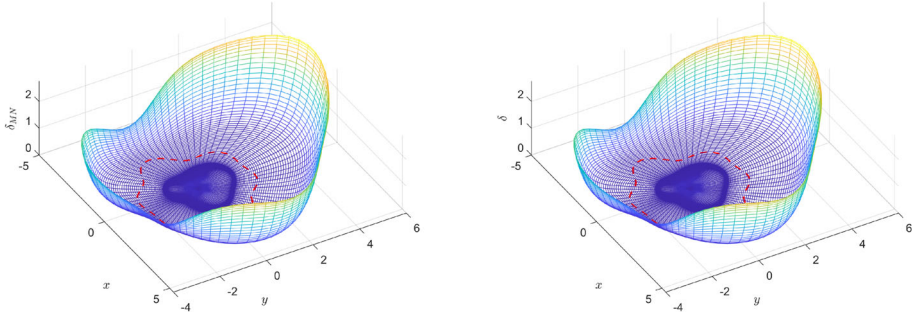

Fig. 13 The images of the reference solution $\delta(x, y)$ (right) and its approximation $\delta_{MN}(x, y)$ (left) with $N = 14$ and $M = 14$

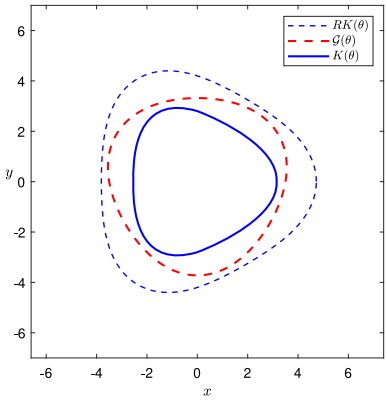

Fig. 14 Diagram illustrating the relationship between the complex interface, boundary, and virtual boundary

We plot the problem geometry in Fig. 14, and present the error curves under various norms in log-log scale for different values of $N = M$ in Fig. 15 which indicates an algebraic convergence.

In Fig. 16, we present the approximate solution and its error with $(N, M) = (18, 18)$.

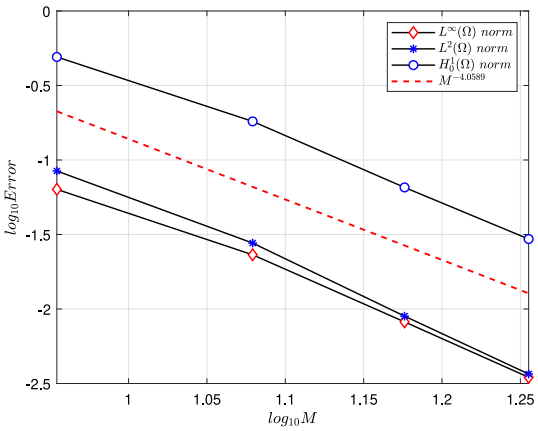

Fig. 15 Error curves under various norms for different values of M and $N = M$

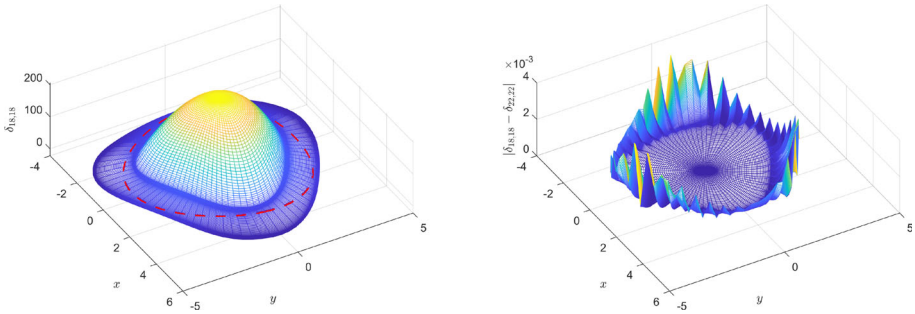

Fig. 16 Plots of approximate solution (left) and error with $(N, M) = (18, 18)$ (right)

7 Conclusions

In this work, we introduced an efficient spectral method for second-order elliptic interface problems in two-dimensional complex domains. The proposed approach features three main attributes:

- It is well-suited for problems involving general heterogeneous media, complex interfaces and complex domains.
- It is based on a fictitious domain approach with circular embedding, transforming the original interface problem in a complex domain to an interface problem in a circular domain in which Fourier-Legendre spectral methods can be efficiently applied.
- For problems with smooth solutions in each subdomains, the resulting algorithm can achieve exponential convergence, requiring significantly fewer degrees of freedom to obtain highly accurate numerical solutions than usual lower-order methods. However, for problems with solutions having limited regularity in each subdomains, our algorithm leads to algebraic convergence rate.

Our numerical results indicate that the discrete Petrov-Galerkin formulation for the elliptic interface problem are well posed. However, how to prove its well-posedness in the discrete and continuous cases is challenging and will be investigated in the future.

The approach proposed in this paper can be extended to problems with multiple layered interfaces. And in principle, the framework developed here can also be extended to three-

dimensional interface problems. These topics will also be the subjects of investigation in the future.

Acknowledgements This research is partially supported by National Natural Science Foundation of China (Grants 12461078, W2431008 and 12371409), Technology Fund of Guizhou Province (Qiankehe Foundation ZK [2024] Key 053).

Funding This work is supported in part by National Natural Science Foundation of China (Grants 12461078, W2431008 and 12371409), Technology Fund of Guizhou Province (Qiankehe Foundation ZK [2024] Key 053).

Data Availability Enquiries about data availability should be directed to the authors.s

Declarations

Ethics Approval This study did not involve any human or animal subjects. Therefore it does not require approval from an ethics committee.

Competing Interests The authors have not disclosed any competing interests.

Conflicts of Interest The authors declare that they have no competing interests.

A Details on the Entries of the Linear System (5.4)

We introduce some symbols as follows:

$$\zeta_{1,1}(t_1,\theta)=\frac{\sin\theta}{r(t_1)K(\theta)},\ \zeta_{2,1}(t_1,\theta)=\frac{\cos\theta}{r(t_1)K(\theta)},\ r\in(0,1);$$
$$\zeta_{1,2}(t_2,\theta)=\frac{\sin\theta}{r(t_2)K(\theta)},\ \zeta_{2,2}(t_2,\theta)=\frac{\cos\theta}{r(t_2)K(\theta)},\ r\in(1,R).$$

Let $D=(-1,1)\times[0,2\pi)$. By substituting the transformation (5.1) into (5.3), we obtain a more explicit form of (5.3):

$$\begin{aligned}
&\int_D(1+t_1)K^2(\theta)\varepsilon_-^*\big[(\xi_1^2+\xi_2^2)\partial_{t_1}\delta_{1N}^M\partial_{t_1}\vartheta_{1N}^M+\frac{1}{2}(\xi_2\zeta_{2,1}-\xi_1\zeta_{1,1})(\partial_{t_1}\delta_{1N}^M\partial_\theta\vartheta_{1N}^M\\
&+\partial_\theta\delta_{1N}^M\partial_{t_1}\vartheta_{1N}^M)+\frac{1}{4}(\zeta_{1,1}^2+\zeta_{2,1}^2)\partial_\theta\delta_{1N}^M\partial_\theta\vartheta_{1N}^M\big]dt_1d\theta\\
&+\int_D(\frac{R+1}{R-1}+t_2)K^2(\theta)\varepsilon_+^*\big[(\xi_1^2+\xi_2^2)\partial_{t_2}\delta_{2N}^M\partial_{t_2}\vartheta_{2N}^M+\frac{R-1}{2}(\xi_2\zeta_{2,2}-\xi_1\zeta_{1,2})\\
&(\partial_{t_2}\delta_{2N}^M\partial_\theta\vartheta_{2N}^M+\partial_\theta\delta_{2N}^M\partial_{t_2}\vartheta_{2N}^M)+\frac{(R-1)^2}{4}(\zeta_{1,2}^2+\zeta_{2,2}^2)\partial_\theta\delta_{2N}^M\partial_\theta\vartheta_{2N}^M\big]dt_2d\theta\\
&=\frac{1}{4}\int_D(1+t_1)K^2(\theta)\mathcal{F}_1\vartheta_{1N}^Mdt_1d\theta+\frac{(R-1)^2}{4}\int_D(\frac{R+1}{R-1}+t_2)K^2(\theta)\mathcal{F}_2\vartheta_{2N}^Mdt_2d\theta,
\end{aligned}\tag{A.1}$$

and

$$\int_D\delta_{2N}^M(\frac{2\mathcal{G}(\theta)}{K(\theta)(R-1)}-\frac{R+1}{R-1},\theta)e^{-in\theta}dt_2d\theta=0,\ |n|\le M,\tag{A.2}$$

where

$$\delta_{iN}^M(t_i,\theta)=\hat{\delta}_{MN}(r(t_i),\theta),\ \vartheta_{iN}^M(t_i,\theta)=\vartheta_{MN}(r(t_i),\theta),\ \mathcal{F}_i(t_i,\theta)=\hat{\mathcal{F}}(r(t_i),\theta),$$
$$\varepsilon_-^*(t_1,\theta)=\hat{\varepsilon}_-(r(t_1),\theta),\ \varepsilon_+^*(t_2,\theta)=\hat{\varepsilon}_+(r(t_2),\theta).$$

Let us denote

$$\Phi_{1,*}(t_1) = \Phi_*(r(t_1)),\ \Phi_{N-1}(t_1) = \Phi_{1,N-1}(r(t_1)),$$
$$\Phi_{2,*}(t_2) = \Phi_*(r(t_2)),\ \hat{\Phi}_{N-1}(t_2) = \Phi_{2,N-1}(r(t_2)),\ \hat{\Phi}_k(t_2) = \Phi_k(t_2).$$

Then, we can expand δ_{1N}^M and δ_{2N}^M as follows:

$$\begin{aligned}\delta_{1N}^M &= \sum_{|m|=0}^{M}[\delta_{*,m}\Phi_{1,*}(t_1) + \sum_{k=0}^{N-1-sign(|m|)}\delta_{1,m}^{(k)}\Phi_k(t_1)]e^{im\theta};\\ \delta_{2N}^M &= \sum_{|m|=0}^{M}[\delta_{*,m}\Phi_{2,*}(t_2) + \sum_{k=0}^{N-1}\delta_{2,m}^{(k)}\hat{\Phi}_k(t_2)]e^{im\theta}.\end{aligned} \tag{A.3}$$

Next, we derive the equivalent matrix form for the discrete formulation (A.1). Firstly, we define the elements of the coefficient matrix that are associated with the internal basis functions, that is,

$$\begin{aligned}a_{n,j}^{m,k} = \int_D (1+t_1)K^2(\theta)\varepsilon_-^*\big[&(\xi_1^2+\xi_2^2)\partial_{t_1}\Phi_k(t_1)\partial_{t_1}\Phi_j(t_1)\\ &+\frac{1}{2}(\xi_2\zeta_{2,1}-\xi_1\zeta_{1,1})[-in\partial_{t_1}\Phi_k(t_1)\Phi_j(t_1)+im\Phi_k(t_1)\partial_{t_1}\Phi_j(t_1)]\\ &+\frac{1}{4}(\zeta_{1,1}^2+\zeta_{2,1}^2)mn\Phi_k(t_1)\Phi_j(t_1)\big]e^{i(m-n)\theta}dt_1d\theta,\end{aligned}$$

and

$$\begin{aligned}b_{n,j}^{m,k} = \int_D (\frac{R+1}{R-1}+t_2)K^2(\theta)\varepsilon_+^*\big[&(\xi_1^2+\xi_2^2)\partial_{t_2}\hat{\Phi}_k(t_2)\partial_{t_2}\Phi_j(t_2)\\ &+\frac{R-1}{2}(\xi_2\zeta_{2,2}-\xi_1\zeta_{1,2})[-in\partial_{t_2}\hat{\Phi}_k(t_2)\Phi_j(t_2)+im\hat{\Phi}_k(t_2)\partial_{t_2}\Phi_j(t_2)]\\ &+\frac{(R-1)^2}{4}(\zeta_{1,2}^2+\zeta_{2,2}^2)mn\hat{\Phi}_k(t_2)\Phi_j(t_2)\big]e^{i(m-n)\theta}dt_2d\theta.\end{aligned}$$

Secondly, we define the elements of the coefficient matrix that are associated with the internal basis functions and interface basis functions, namely,

$$\begin{aligned}c_{1,n}^{m,k} = \int_D (1+t_1)K^2(\theta)\varepsilon_-^*\big[&(\xi_1^2+\xi_2^2)\partial_{t_1}\Phi_k(t_1)\partial_{t_1}\Phi_{1,*}(t_1)\\ &+\frac{1}{2}(\xi_2\zeta_{2,1}-\xi_1\zeta_{1,1})[-in\partial_{t_1}\Phi_k(t_1)\Phi_{1,*}(t_1)+im\Phi_k(t_1)\partial_{t_1}\Phi_{1,*}(t_1)]\\ &+\frac{1}{4}(\zeta_{1,1}^2+\zeta_{2,1}^2)mn\Phi_k(t_1)\Phi_{1,*}(t_1)\big]e^{i(m-n)\theta}dt_1d\theta,\\ c_{2,n}^{m,k} = \int_D (\frac{R+1}{R-1}+t_2)K^2(\theta)\varepsilon_+^*\big[&(\xi_1^2+\xi_2^2)\partial_{t_2}\hat{\Phi}_k(t_2)\partial_{t_2}\Phi_{2,*}(t_2)\\ &+\frac{R-1}{2}(\xi_2\zeta_{2,2}-\xi_1\zeta_{1,2})[-in\partial_{t_2}\hat{\Phi}_k(t_2)\Phi_{2,*}(t_2)+im\hat{\Phi}_k(t_2)\partial_{t_2}\Phi_{2,*}(t_2)]\\ &+\frac{(R-1)^2}{4}(\zeta_{1,2}^2+\zeta_{2,2}^2)mn\hat{\Phi}_k(t_2)\Phi_{2,*}(t_2)\big]e^{i(m-n)\theta}dt_2d\theta;\end{aligned}$$

and

$$d_{1,m}^{n,j} = \int_D (1+t_1)K^2(\theta)\varepsilon_-^*\big[(\xi_1^2+\xi_2^2)\partial_{t_1}\Phi_{1,*}(t_1)\partial_{t_1}\Phi_j(t_1)$$

$$
\begin{aligned}
&+\frac{1}{2}(\xi_2\zeta_{2,1}-\xi_1\zeta_{1,1})[-in\partial_{t_1}\Phi_{1,*}(t_1)\Phi_j(t_1)+im\Phi_{1,*}(t_1)\partial_{t_1}\Phi_j(t_1)]\\
&+\frac{1}{4}(\zeta_{1,1}^2+\zeta_{2,1}^2)mn\Phi_{1,*}(t_1)\Phi_j(t_1)\Big]e^{i(m-n)\theta}dt_1d\theta,\\
d_{2,m}^{n,j}=&\int_D(\frac{R+1}{R-1}+t_2)K^2(\theta)\varepsilon_+^*\Big[(\xi_1^2+\xi_2^2)\partial_{t_2}\Phi_{2,*}(t_2)\partial_{t_2}\Phi_j(t_2)\\
&+\frac{R-1}{2}(\xi_2\zeta_{2,2}-\xi_1\zeta_{1,2})[-in\partial_{t_2}\Phi_{2,*}(t_2)\Phi_j(t_2)+im\Phi_{2,*}(t_2)\partial_{t_2}\Phi_j(t_2)]\\
&+\frac{(R-1)^2}{4}(\zeta_{1,2}^2+\zeta_{2,2}^2)mn\Phi_{2,*}(t_2)\Phi_j(t_2)\Big]e^{i(m-n)\theta}dt_2d\theta.
\end{aligned}
$$

Thirdly, we define the elements of the coefficient matrix that are associated with the interface basis functions, namely,

$$
\begin{aligned}
\epsilon_1^{mn}=&\int_D(1+t_1)K^2(\theta)\varepsilon_-^*\Big[(\xi_1^2+\xi_2^2)\partial_{t_1}\Phi_{1,*}(t_1)\partial_{t_1}\Phi_{1,*}(t_1)\\
&+\frac{1}{2}(\xi_2\zeta_{2,1}-\xi_1\zeta_{1,1})[-in\partial_{t_1}\Phi_{1,*}(t_1)\Phi_{1,*}(t_1)+im\Phi_{1,*}(t_1)\partial_{t_1}\Phi_{1,*}(t_1)]\\
&+\frac{1}{4}(\zeta_{1,1}^2+\zeta_{2,1}^2)mn\Phi_{1,*}(t_1)\Phi_{1,*}(t_1)\Big]e^{i(m-n)\theta}dt_1d\theta,\\
\epsilon_2^{mn}=&\int_D(\frac{R+1}{R-1}+t_2)K^2(\theta)\varepsilon_+^*\Big[(\xi_1^2+\xi_2^2)\partial_{t_2}\Phi_{2,*}(t_2)\partial_{t_2}\Phi_{2,*}(t_2)\\
&+\frac{R-1}{2}(\xi_2\zeta_{2,2}-\xi_1\zeta_{1,2})[-in\partial_{t_2}\Phi_{2,*}(t_2)\Phi_{2,*}(t_2)+im\Phi_{2,*}(t_2)\partial_{t_2}\Phi_{2,*}(t_2)]\\
&+\frac{(R-1)^2}{4}(\zeta_{1,2}^2+\zeta_{2,2}^2)mn\Phi_{2,*}(t_2)\Phi_{2,*}(t_2)\Big]e^{i(m-n)\theta}dt_2d\theta.
\end{aligned}
$$

Finally, we define the elements related to the constraint conditions, namely,

$$
\begin{aligned}
z_n^{m,k}&=\int_0^{2\pi}\hat{\Phi}_k(\frac{2\mathcal{G}(\theta)}{K(\theta)(R-1)}-\frac{R+1}{R-1})e^{i(m-n)\theta}d\theta,\\
\varpi_{mn}&=\int_0^{2\pi}\Phi_{2,*}(\frac{2\mathcal{G}(\theta)}{K(\theta)(R-1)}-\frac{R+1}{R-1})e^{i(m-n)\theta}d\theta.
\end{aligned}
$$

Next, we will proceed to define the elements in the right-hand vector, specifically,

$$
\begin{aligned}
f_{1,j,n}&=\frac{1}{4}\int_D(1+t_1)K^2(\theta)\mathcal{F}_1\Phi_j(t_1)e^{-in\theta}dt_1d\theta,\\
f_{2,j,n}&=\frac{(R-1)^2}{4}\int_D(\frac{R+1}{R-1}+t_2)K^2(\theta)\mathcal{F}_2\Phi_j(t_2)e^{-in\theta}dt_2d\theta,\\
f_{*,n}&=\frac{1}{4}\int_D(1+t_1)K^2(\theta)\mathcal{F}_1\Phi_{1,*}(t_1)e^{-in\theta}dt_1d\theta\\
&\quad+\frac{(R-1)^2}{4}\int_D(\frac{R+1}{R-1}+t_2)K^2(\theta)\mathcal{F}_2\Phi_{2,*}(t_2)e^{-in\theta}dt_2d\theta.
\end{aligned}
$$

By substituting (A.3) into (A.1) and (A.2), and taking ϑ_{MN} across all basis functions in X_{MN}, we find that (A.1) and (A.2), i.e., (5.4) can be written as the following matrix form:

$$\begin{bmatrix} \mathcal{H}_{-M}^{-M} & \cdots & \mathcal{H}_{-M}^{0} & \cdots & \mathcal{H}_{-M}^{M} \\ \vdots & \ddots & \vdots & \ddots & \vdots \\ \mathcal{H}_{0}^{-M} & \cdots & \mathcal{H}_{0}^{0} & \cdots & \mathcal{H}_{0}^{M} \\ \vdots & \ddots & \vdots & \ddots & \vdots \\ \mathcal{H}_{M}^{-M} & \cdots & \mathcal{H}_{M}^{0} & \cdots & \mathcal{H}_{M}^{M} \\ S_{-M}^{-M} & \cdots & S_{-M}^{0} & \cdots & S_{-M}^{M} \\ \vdots & \ddots & \vdots & \ddots & \vdots \\ S_{0}^{-M} & \cdots & S_{0}^{0} & \cdots & S_{0}^{M} \\ \vdots & \ddots & \vdots & \ddots & \vdots \\ S_{M}^{-M} & \cdots & S_{M}^{0} & \cdots & S_{M}^{M} \end{bmatrix} \begin{bmatrix} U^{-M} \\ \vdots \\ U^{0} \\ \vdots \\ U^{M} \end{bmatrix} = \begin{bmatrix} Y_{-M} \\ \vdots \\ Y_0 \\ \vdots \\ Y_M \\ 0 \\ \vdots \\ 0 \\ \vdots \\ 0 \end{bmatrix}, \tag{A.4}$$

where

$$\mathcal{H}_n^m = \begin{bmatrix} A_n^m & \mathbf{0} & D_{1,n,m} \\ \mathbf{0} & B_n^m & D_{2,n,m} \\ C_{1,m,n} & C_{2,m,n} & \epsilon_1^{mn} + \epsilon_2^{mn} \end{bmatrix}, \ S_n^m = [\mathbf{0}, Z_{mn}, \varpi_{mn}],$$
$$U^m = [U^{1,m}, U^{2,m}, \delta_{*,m}]^T, \ Y_n = [Y_{1,n}, Y_{2,n}, f_{*,n}]^T,$$

and

$$A_n^m = (a_{n,j}^{m,k}), \ B_n^m = (b_{n,j}^{m,k}), \ C_{1,m,n} = (c_{1,n}^{m,0}, \ldots, c_{1,n}^{m,N-1-sign(|m|)}),$$
$$C_{2,m,n} = (c_{2,n}^{m,0}, \ldots, c_{2,n}^{m,N-1}), \ D_{1,n,m} = (d_{1,m}^{n,0}, \ldots, d_{1,m}^{n,N-1-sign(|n|)})^T,$$
$$D_{2,n,m} = (d_{2,m}^{n,0}, \ldots, d_{2,m}^{n,N-2})^T, \ Z_{mn} = (z_n^{m,0}, \ldots, z_n^{m,N-1}),$$
$$U^{1,m} = [\delta_{1,m}^{(0)}, \ldots, \delta_{1,m}^{(N-1-sign(|m|))}], \ U^{2,m} = [\delta_{2,m}^{(0)}, \ldots, \delta_{2,m}^{(N-1)}],$$
$$Y_{1,n} = [f_{1,0,n}, \ldots, f_{1,N-1-sign(|n|),n}], \ Y_{2,n} = [f_{2,0,n}, \ldots, f_{2,N-2,n}].$$

References

1. Adjerid, S., Lin, T., Meghaichi, H.: A high order geometry conforming immersed finite element for elliptic interface problems. Comput. Methods Appl. Mech. Eng. **420**, 116703 (2024)
2. Badia, S., Codina, R.: A combined nodal continuous-discontinuous finite element formulation for the maxwell problem. Appl. Math. Comput. **218**(8), 4276–4294 (2011)
3. Banks, H.T., Buksas, M.W., Lin, T.: Electromagnetic material interrogation using conductive interfaces and acoustic wavefronts. Society for Industrial and Applied Mathematics, (2000)
4. Beale, T., Layton, A.: On the accuracy of finite difference methods for elliptic problems with interfaces. Commun. Appl. Math. Comput. Sci. **1**(1), 91–119 (2007)
5. Brenner, S.C., Scott, L.R.: The mathematical theory of finite element methods. Springer, New York (2008)
6. Canuto, C., Hussaini, M.Y., Quarteroni, A., Zang, T.A.: Spectral methods: fundamentals in single domains. Springer-Verlag, Berlin (2006)
7. Canuto, C., Hussaini, M.Y., Quarteroni, A., Zang, T.A.: Spectral methods: evolution to complex geometries and applications to fluid dynamics. Springer, Berlin (2007)
8. Waixiang Cao, X., Zhang, Z.Z., Zou, Q.: Superconvergence of immersed finite volume methods for one-dimensional interface problems. J. Sci. Comput. **73**(2), 543–565 (2017)
9. Chen, Z., Zou, J.: Finite element methods and their convergence for elliptic and parabolic interface problems. Numer. Math. **79**(2), 175–202 (1998)

10. Coco, A., Russo, G.: Second order finite-difference ghost-point multigrid methods for elliptic problems with discontinuous coefficients on an arbitrary interface. J. Comput. Phys. **361**, 299–330 (2018)
11. Davydov, O., Safarpoor, M.: A meshless finite difference method for elliptic interface problems based on pivoted qr decomposition. Appl. Numer. Math. **161**, 489–509 (2021)
12. Deka, B., Ahmed, T.: Convergence of finite element method for linear second-order wave equations with discontinuous coefficients. Numer. Methods Partial Differ. Equations **29**(5), 1522–1542 (2013)
13. Dülk, I., Kovácsházy, T.: Steady-state heat conduction in multilayer bodies: An analytical solution and simplification of the eigenvalue problem. Int. J. Heat Mass Transfer **67**, 784–797 (2013)
14. Ewing, R.E., Li, Z., Lin, T., Lin, Y.: The immersed finite volume element methods for the elliptic interface problems. Math. Comput. Simul. **50**(1–4), 63–76 (1999)
15. Ewing, R.E., Lin, T., Lin, Y.: On the accuracy of the finite volume element method based on piecewise linear polynomials. SIAM J. Numer. Anal. **39**(6), 1865–1888 (2002)
16. Yiqi, G., Shen, J.: An efficient spectral method for elliptic pdes in complex domains with circular embedding. SIAM J. Sci. Comput. **43**(1), A309–A329 (2021)
17. Yiqi, G., Shen, J.: A fictitious domain spectral method for solving the helmholtz equation in exterior domains. J. Sci. Comput. **94**(3), 46 (2023)
18. Guittet, A., Lepilliez, M., Tanguy, S., Gibou, F.: Solving elliptic problems with discontinuities on irregular domains-the voronoi interface method. J. Comput. Phys. **298**, 747–765 (2015)
19. Guo, R., Lin, T.: An immersed finite element method for elliptic interface problems in three dimensions. J. Comput. Phys. **414**, 109478 (2020)
20. He, X., Lin, T., Lin, Y.: A bilinear immersed finite volume element method for the diffusion equation with discontinuous coefficient. Commun. Comput. Phys. **6**(1), 185 (2009)
21. Hiptmair, R., Li, J., Zou, J.: Convergence analysis of finite element methods for h (curl; ω)-elliptic interface problems. Numer. Math. **122**(3), 557–578 (2012)
22. Ji, H., Weng, Z., Zhang, Q.: An augmented immersed finite element method for variable coefficient elliptic interface problems in two and three dimensions. J. Comput. Phys. **418**, 109631 (2020)
23. Khan, A., Husain, A., Mohapatra, S., Upadhyay, C.S.: Spectral element method for three dimensional elliptic problems with smooth interfaces. Comput. Methods Appl. Mech. Eng. **315**, 522–549 (2017)
24. Kishore Kumar, N., Naga Raju, G.: Nonconforming least-squares method for elliptic partial differential equations with smooth interfaces. J. Sci. Comput. **53**(2), 295–319 (2012)
25. LeVeque, R.J., Li, Z.: The immersed interface method for elliptic equations with discontinuous coefficients and singular sources. SIAM J. Numer. Anal. **31**(4), 1019–1044 (1994)
26. Li, J., Jiang, Y.: Stable generalized finite element for two-dimensional and three-dimensional non-homogeneous interface problems. Appl. Math. Comput. **486**, 129056 (2025)
27. Li, Z.: The immersed interface method: A numerical approach for partial differential equations with interfaces. University of Washington, (1994)
28. Li, Z.: A note on immersed interface method for three-dimensional elliptic equations. Comput. Math. Appl. **31**(3), 9–17 (1996)
29. Li, Z.: A fast iterative algorithm for elliptic interface problems. SIAM J. Numer. Anal. **35**(1), 230–254 (1998)
30. Li, Z.: The immersed interface method using a finite element formulation. Appl. Numer. Math. **27**(3), 253–267 (1998)
31. Li, Z., Lin, T., Lin, Y., Rogers, R.C.: An immersed finite element space and its approximation capability. Num. Methods Partial Differ. Equ. **20**(3), 338–367 (2004)
32. Lin, T., Lin, Y., Zhang, X.: Partially penalized immersed finite element methods for elliptic interface problems. SIAM J. Numer. Anal. **53**(2), 1121–1144 (2015)
33. Lin, M., Wang, J., Ye, X., Zhao, S.: A new weak galerkin finite element method for elliptic interface problems. J. Comput. Phys. **325**, 157–173 (2016)
34. Oruç, Ö.: An efficient meshfree method based on pascal polynomials and multiple-scale approach for numerical solution of 2-d and 3-d second order elliptic interface problems. J. Comput. Phys. **428**, 110070 (2021)
35. Pan, K., He, D., Li, Z.: A high order compact fd framework for elliptic bvps involving singular sources, interfaces, and irregular domains. J. Sci. Comput. **88**(3), 67 (2021)
36. Plexousakis, M., Zouraris, G.E.: On the construction and analysis of high order locally conservative finite volume-type methods for one-dimensional elliptic problems. SIAM J. Numer. Anal. **42**(3), 1226–1260 (2004)
37. Shen, J., Tang, T., Wang, L.L.: Spectral methods: algorithms, analysis and applications, vol. 41. Springer-Berlin, Heidelberg (2011)
38. Süli, E.: Convergence of finite volume schemes for poisson's equation on nonuniform meshes. SIAM J. Numer. Anal. **28**(5), 1419–1430 (1991)

39. Wang, C., Wang, Z., Wang, Z.: An efficient spectral method for singularly perturbed convection-diffusion-reaction problems in three-dimensional irregular exterior domains. J. Sci. Comput. **105**(1), 31 (2025)
40. Wang, Q., Zhang, Z., Wang, L.: New immersed finite volume element method for elliptic interface problems with non-homogeneous jump conditions. J. Comput. Phys. **427**, 110075 (2021)
41. Wang, Z., Wen, X., Yao, G.: An efficient spectral-galerkin method for elliptic equations in 2d complex geometries. J. Sci. Comput. **95**(3), 89 (2023)
42. Xing, Y., Song, L., He, X., Qiu, C.: A generalized finite difference method for solving elliptic interface problems. Math. Comput. Simul. **178**, 109–124 (2020)
43. Yao, G., Wen, X., Wang, Z.: Efficient spectral methods for pdes in three-dimensional curved geometries. J. Sci. Comput. **103**(3), 95 (2025)
44. Zhang, C., LeVeque, R.J.: The immersed interface method for acoustic wave equations with discontinuous coefficients. Wave Motion **25**(3), 237–263 (1997)
45. Zhang, Q., Ito, K., Li, Z., Zhang, Z.: Immersed finite elements for optimal control problems of elliptic pdes with interfaces. J. Comput. Phys. **298**, 305–319 (2015)
46. Ray Zirui Zhang and Li-Tien Cheng: A compact coupling interface method with second-order gradient approximation for elliptic interface problems. J. Sci. Comput. **100**(2), 32 (2024)
47. Zhu, L., Zhang, Z., Li, Z.: An immersed finite volume element method for 2d pdes with discontinuous coefficients and non-homogeneous jump conditions. Comput. Math. Appl. **70**(2), 89–103 (2015)